Computational Materials Science 215 (2022) 111775

Contents lists available at ScienceDirect

Computational Materials Science

journal homepage: www.elsevier.com/locate/commatsci

Full length article

Uncertainty quantification of metallic microstructures using principal image moments

Arulmurugan Senthilnathan [a], Iman Javaheri [b,c], Hengduo Zhao [a], Veera Sundararaghavan [c], Marc DeGraef [d], Pınar Acar [a,*]

[a] Department of Mechanical Engineering, Virginia Tech, Blacksburg, VA, 24060, USA
[b] NASA Langley Research Center, Hampton, 23666, VA, USA
[c] Department of Aerospace Engineering, University of Michigan, Ann Arbor, 48109, MI, USA
[d] Department of Materials Science and Engineering, Carnegie Mellon University, Pittsburgh, 15213, PA, USA

ARTICLE INFO

Keywords:
Microstructure reconstruction
Uncertainty quantification
Shape moment
Gaussian process

ABSTRACT

The present work uses Markov Random Field (MRF) algorithm to construct large-scale and statistically-equivalent samples from small-scale experimental data of metallic microstructures. While the MRF method can build such digital material representations in large computational domains, its algorithmic stochasticity (epistemic uncertainty) causes variations in the resulting microstructural features, such as the texture and grain topology. This work addresses the effects of the epistemic uncertainty on homogenized mechanical properties by characterizing the variations in the microstructural features using a shape descriptor based on the concept of moment invariants. In particular, 2D and 3D synthetic microstructure data for Titanium-7wt%Aluminum (Ti-7Al) alloy is generated with the MRF method using smaller-scale 2D experimental data. To quantify the uncertainty of the reconstructed synthetic samples, a graphical method and five different metrics of statistical variability are developed. Next, the propagation of the microstructural uncertainty on homogenized properties is studied using an analytical uncertainty quantification (UQ) algorithm and Gaussian Process Regression (GPR).

1. Introduction

Microstructure reconstruction techniques have rapidly evolved over the past few years as they can save the cost and time required for purely experimental approaches to characterize microstructure information in large domains. Some of these techniques include two point correlations either with simulated annealing [1–6] or phase recovery algorithm [7,8], ellipsoid or geometric distribution based reconstruction [4,9], Support Vector Machine (SVM) [10], Markov Random Field (MRF) [11–15], machine learning [16–20], image inpainting [21], experimental reconstruction through milling [22,23]and Voronoi tessellation [24,25]. All image-based reconstruction techniques aim to generate statistically-equivalent synthetic microstructure representations. However, they do not account for the variability arising from the algorithmic uncertainty that affects the synthesized microstructures and thus the homogenized material properties.

There are two classes of microstructural uncertainty. The first class is the aleatoric uncertainty that is related to the lack of knowledge for identifying the correct pixel intensity information in the EBSD image. The second class, epistemic uncertainty, arises from inherent randomness in the MRF algorithm. Both aleatoric and epistemic uncertainty can propagate on material properties and alter the expected performance of components. To improve the reliability and performance of materials, it is crucial to understand the effects of the uncertainty. The present work investigates the epistemic uncertainty associated with computational microstructure reconstruction to understand its effects on homogenized mechanical properties of metallic alloys.

Although there are previous efforts to quantify crystallographic texture uncertainty [26–30], the impacts of the microstructure uncertainty on grain shapes are not extensively studied to the best of the authors' knowledge. The characterization and quantification of grain shapes of polycrystalline microstructures are significant to understand the effects of the uncertainty on different grain shapes and homogenized properties.

The quantification of grain shapes is challenging due to a wide variety and complexity of possible grain shapes, including highly non-convex or concave grains [31]. Many practical methods to quantify

* Corresponding author.
E-mail address: pacar@vt.edu (P. Acar).

https://doi.org/10.1016/j.commatsci.2022.111775
Received 8 May 2022; Received in revised form 16 August 2022; Accepted 26 August 2022
Available online 23 September 2022

the grain shapes were based on intuitive approaches involving experiments [32,33]. For example, the widely-used two-point correlations [34–36] provide implicit information of the grain shapes. A similar yet more informative descriptor is the 2 point cluster correlation which can be used to quantify the microstructure in 3D domains as well [37]. However, they do not explicitly determine the size and shape of individual grains [38]. Unlike point based functions, line based comparisons are also attempted [13,16] using linear path functions which do not cover entire microstructure both in 2D and 3D domains. Geometrical shape based descriptors are introduced for quantifying grain shapes [18,37]. However, these descriptors are not ideal for quantifying complex grain shapes, such as those arising from additively manufactured microstructures. The shape quotient is another measure that is used to capture the grain shape of common geometries [39]. Nevertheless, none of the shape descriptors and correlation functions discussed above explicitly capture the shape. Therefore, they cannot be used as a universal metric to characterize the uncertainty of different grains.

The application of moment invariants for measuring shapes has also been investigated to quantify grain shapes of 2-D and 3-D microstructures. [40–48]. MacSleyne et al. [44] discussed the applications of dimensionless moment invariants (denoted by ω_1 and ω_2) and introduced normalized moments as a shape descriptor, specifically for 3D microstructures [45,46]. In addition, MacSleyne et al. [45] have derived a moment invariant formulation for each geometrical shape such as a circle, square, rectangle, and introduced moment invariant density maps plotted for both 2D [45] and 3D shapes [43]. Their application includes a range of studies including classification of particle shapes [42], comparison of experimental and synthetic grains [45], and quantification and analysis of precipitate shapes [45,46,49] through common geometric shapes. While these methods work well for not-so-complex grain shapes, the highly irregular grain shapes of the additively manufactured materials cannot be quantified by these techniques as they may significantly differ from standard geometries. To address this problem, the present study aims to quantify the grain shapes of microstructures without the need of comparing them to another geometry.

The presented strategy is based upon the use of the moment invariants. We explore different measures to quantify the effects of the uncertainty in 2D and 3D grain shapes of microstructures using these descriptors. The moment invariants were initially formulated by Hu as a special set of image moments that are invariant to translation, scale, and rotation [50]. In particular, these moments are a measure of the pixel intensity of an image with respect to the location as they describe the distribution of the pixel intensities over the image. They have applications in multiple disciplines, ranging from a simple object shape detection to the human face recognition [51–56]. For instance, Žunić [57–60] studied the application of the first Hu moment to measure the circularity, ellipticity, and ellipsoidness of 2D and 3D shapes.

The image moments have been applied before in our previous work [61] to compare experimental and synthesized 2D microstructure images at global and local levels. The present work proposes to use the concept of moment invariants to study the uncertainty propagation on the grain features of 2D or 3D synthetic microstructures. This objective is achieved by developing a graphical method using principal eigenvalue moments (PEM). The development of such graphical approach is advantageous for deriving different statistical parameters that can measure the uncertainty of microstructural texture and topology.

Many state-of-the-art models have been developed for uncertainty quantification (UQ) using numerical and analytical techniques [26,62–66]. The numerical UQ algorithms pose some challenges. For instance, the Monte Carlo Simulation (MCS) is a computationally expensive method that can be numerically intractable for quantifying the uncertainty of large 3D microstructure samples [62]. As an alternative strategy, surrogate models have been developed using machine learning (ML) techniques [65]. While these methods demonstrate significant promise, the image-based ML methods require substantial amounts of data. Therefore, the present study explores the effects of the epistemic uncertainty on grain shapes and resulting homogenized properties of microstructures by utilizing an analytical UQ method and a Gaussian Process Regression (GPR)-based surrogate model that is parametrically developed in terms of the moment invariants. The organization of the paper is as follows. Section 2 explains the methodology behind the MRF algorithm. Section 3 discusses the concept of moment invariants. Section 4 addresses uncertainty quantification for 2D-to-2D microstructure reconstruction and introduces new statistical parameters. Section 5 explains the extension of the presented methodology in Section 4 to 3D microstructures. Section 6 discusses the propagation of the uncertainty on homogenized mechanical properties.

2. Microstructure reconstruction using MRFs

The Markov Random Field (MRF) method is applied in this work to reconstruct the microstructures of Ti-7Al alloy in 2D and 3D domains. A brief explanation about the concept of MRF, studied previously [13,61], is provided next.

The MRF is related to the concept of a probabilistic graphical model which is constructed from a set of Random Variables (RV) based on their conditional dependence. There are two categories of probabilistic graphical models: Directed Graphical Model (DGM) and Undirected Graphical Model (UGM). The difference between both of them lies in assigning a direction to the edges connecting two random variables. A classical example of a directed model is the Bayesian network where each RV depends on the previous one. However, due to the absence of a direction, a neighborhood analysis is defined in the undirected models. Conventionally, the UGM is also known as Markov networks. The graphical network is designed in a way to have conditional dependence on each pixel's neighbors exhibiting a joint probability distribution globally throughout the image. Due to the resemblance of Markov networks to a lattice-based constructed model, MRF is represented by an Ising model [67] where the joint probability density of all particles is defined by the local Markovian property. In an Ising model, each particle, representing the pixels, conditionally depends on its neighbors. In other words, the edge connecting two particles of the lattice is absent if they both are conditionally independent. The joint probability of directed models has a dependency on its previous state whereas the joint probability indicating the edges connecting two variables in the MRF is represented by a potential function. Markovian property states that the probability of a value (X) is conditionally independent of all other values that are placed outside of its neighbors. When this method is applied to an image, each particle represents a pixel of the image while the value represents the pixel intensity. More information on MRF can be found in [13]. This approach is implemented to reconstruct a simple cobblestone image and the microstructures of the Ti-7Al alloy produced by forging and additive manufacturing. The samples are reconstructed both in 2D (Fig. 1) and 3D (Fig. 4) domains and the microstructural uncertainty is quantified using five different parameters based on Hu moments.

3. Statistical meaning and significance of Hu moments

Hu moments are defined as the set of seven invariant numbers for shape transformations (Eqs. (1)–(7)). The first two Hu moments are the second-order moments, whereas the remaining functions are purely of third-order moments, except the fiveth Hu moment, which has both second and third-order terms. They are invariant to translation, rotation, and scale, which is a useful feature for applications in diverse fields [51–53]. They are used not only to identify a shape in an image but also to capture a pattern [50].

$$\phi_1 = \eta_{20} + \eta_{02} \tag{1}$$

$$\phi_2 = (\eta_{20} - \eta_{02})^2 + 4\eta_{11}^2 \tag{2}$$

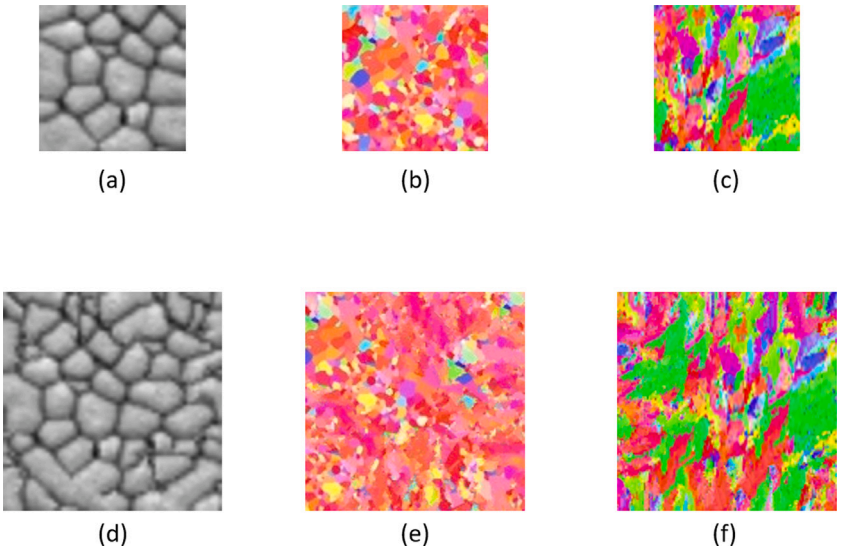

Fig. 1. Original experimental images of (a) Cobblestone of size 36 × 36, (b) Forged Ti-7Al of size 100 × 100, (c) Additively manufactured material of size 93 × 93, (d) Reconstructed example of the cobblestone image with resolution 56 × 56, (e) Reconstructed example of the forged Ti-7Al with resolution 150 × 150, and (f) Reconstructed example of the additively manufactured material with resolution 140 × 140.

$$\phi_3 = (\eta_{30} - 3\eta_{12})^2 + (3\eta_{21} - \eta_{03})^2 \tag{3}$$

$$\phi_4 = (\eta_{30} + \eta_{12})^2 + (\eta_{21} + \eta_{03})^2 \tag{4}$$

$$\begin{aligned}\phi_5 = {} & (\eta_{30} - 3\eta_{12})(\eta_{30} + \eta_{12})[(\eta_{30} + \eta_{12})^2 - 3(\eta_{21} + \eta_{03})^2] \\ & + (3\eta_{21} - \eta_{03})(\eta_{21} + \eta_{03})[3(\eta_{30} + \eta_{12})^2 - (\eta_{21} + \eta_{03})^2]\end{aligned} \tag{5}$$

$$\begin{aligned}\phi_6 = {} & (\eta_{20} - \eta_{02})[(\eta_{30} + \eta_{12})^2 - (\eta_{21} + \eta_{03})^2] \\ & + 4\eta_{11}[(\eta_{30} + \eta_{12})(\eta_{21} + \eta_{03})]\end{aligned} \tag{6}$$

$$\begin{aligned}\phi_7 = {} & (3\eta_{21} - \eta_{03})(\eta_{30} + \eta_{12})[(\eta_{30} + \eta_{12})^2 - 3(\eta_{21} \\ & + \eta_{03})^2] - (\eta_{30} - 3\eta_{12})(\eta_{21} + \eta_{03})[3(\eta_{30} + \eta_{12})^2 \\ & - (\eta_{21} + \eta_{03})^2]\end{aligned} \tag{7}$$

These seven Hu moments consist of normalized central moments (Eq. (8)), which are defined as the ratio of central moments (Eq. (9)) to the image area. The central moments are statistically equivalent to the variance.

$$\eta_{ij} = \frac{\mu_{ij}}{(m_{00})^{\gamma}} \text{ where } \gamma = \frac{2 + i + j}{2} \tag{8}$$

$$\mu_{ij} = \sum_x \sum_y (x - \bar{x})^i (y - \bar{y})^j I(x, y) \tag{9}$$

where $\bar{x}$ and $\bar{y}$ are the (x, y) coordinates of the centroid of the image, and I(x, y) represents the pixel intensity value.

The central moments are developed in the form of multi-variate distributions. Hence, the second-order central moments represent the covariance (μ_{20}, μ_{02}, μ_{11}) of an image while the third-order normalized central moment contains the skewness information of the same image. Similarly, a fourth-order moment would provide information about the kurtosis of the image. The present work focuses on the utilization of the second-order Hu moments, which are used to quantify the grain shapes. Interested readers are referred to [68] for more information about the statistical meaning of the higher order Hu moments.

By calculating all the second-order central moments, the covariance matrix can be formed as:

$$\begin{bmatrix} \Sigma_{xx} & \Sigma_{xy} \\ \Sigma_{xy} & \Sigma_{yy} \end{bmatrix} = \begin{bmatrix} \mu_{20} & \mu_{11} \\ \mu_{11} & \mu_{02} \end{bmatrix} \tag{10}$$

Similarly, a 2 × 2 covariance matrix for the normalized central moments can be defined as:

$$\begin{bmatrix} \eta_{20} & \eta_{11} \\ \eta_{11} & \eta_{02} \end{bmatrix} \tag{11}$$

The eigenvalues can be formulated in terms of the Hu moments, as follows:

$$\lambda_{1/2} = \frac{\phi_1 \pm \sqrt{\phi_2}}{2} \tag{12}$$

The present work uses the Principal Eigenvalue Moments (PEM) based graphical domain to derive five parameters to quantify the uncertainty arising from the reconstruction of 2D and 3D microstructures. A similar approach was presented earlier [44,45] with a map of ω_1 and ω_2 for comparing grain shapes. Here, ω_1 and ω_2 are the dimensionless moment invariants. The map developed from these moments can be used to characterize the grain and particle shapes. However, in this work, the focus is on quantifying the uncertainty propagated on the reconstructed microstructures with a map of PEM. Furthermore, the PEM map can be used as a universal measure for understanding the uncertainty propagated on both 2D and 3D reconstructed microstructures.

4. Uncertainty quantification for 2D-to-2D microstructure reconstruction

Three different images are used to predict the larger scale evolution of microstructures. While two of these images (Fig. 1(b) and (c)) show the Ti-7Al microstructure samples produced by forging and additive manufacturing, a cobblestone sample (Fig. 1(a)) is also used to compare its results to other microstructures. Using the MRF method, a total of 1000 images are reconstructed for each image. Fig. 1 (d-f) shows one example selected among 1000 synthesized images. The probability of finding the optimum pixel intensity value for the synthetic structure is achieved through a Gaussian distributed weight parameter by the MRF algorithm [13]. The synthesized microstructure texture quantified by the PEM has also yielded a similar probability distribution (Fig. 2). The advantage of the Gaussian distribution feature is taken for modeling the uncertainty of material properties. The absolute PEMs are calculated for the whole image and their values are plotted (Fig. 3) in natural logarithmic scale. Fig. 3 shows the $\ln|\lambda|$ values of both experimental and synthetic microstructures. Here, the synthetic data (represented with λ_s) forms a cluster around the experimental eigenvalue (λ_e). The

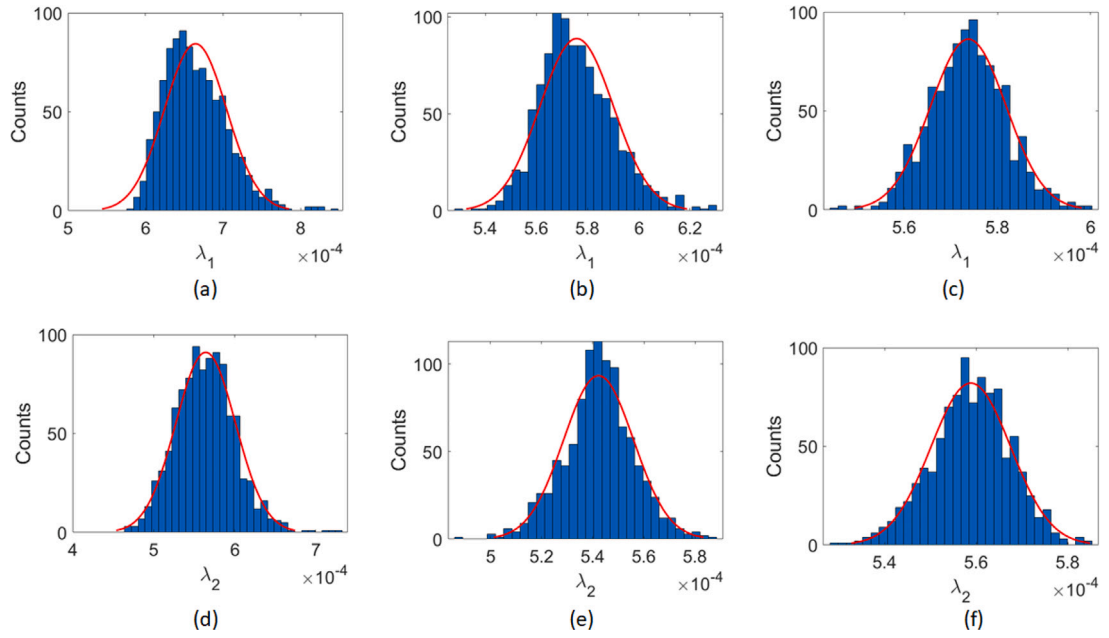

Fig. 2. (a)–(c) Standard normal distributions of λ_1 for additively manufactured Ti-7Al microstructure, forged Ti-7Al microstructure, and cobblestone sample, (d)–(f) Standard normal distributions of λ_2 for additively manufactured Ti-7Al microstructure, forged Ti-7Al microstructure, and cobblestone sample.

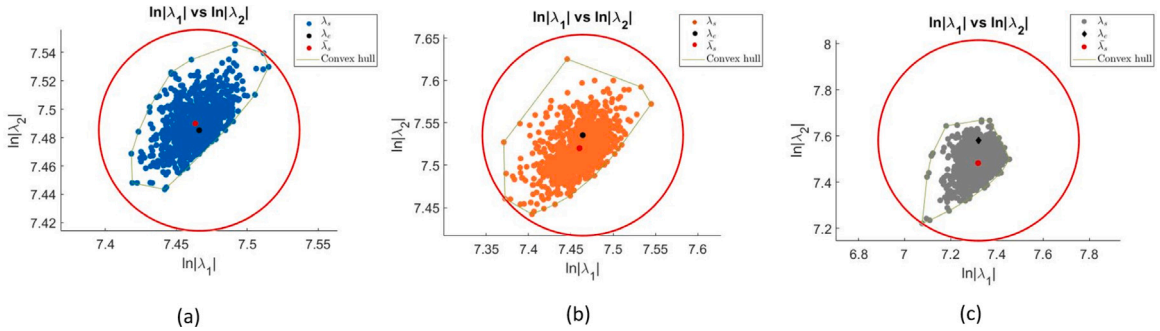

Fig. 3. PEM based Map for (a) Cobblestone (b) Forged Ti-7Al microstructure, (c) Additively manufactured Ti-7Al microstructure.

Table 1
Parameters to statistically validate 2D images.

	R	d_λ	ζ	ρ_a	ρ_p
Cobblestone	0.0708	0.0055	0.0186	2.9417	1.4678
Forged	0.1187	0.0159	0.0336	2.3579	1.3828
Additively manufactured	0.4348	0.0981	0.1186	5.8036	2.1048

eigenvalues are calculated using Eq. (12) for any particular image. While λ_e is constant for a single experimental image, λ_s varies within $\lambda_{s1}, \lambda_{s2}, \ldots, \lambda_{sN}$ for the synthetic images ranging from 1 to N, where N represents the total number of reconstructed samples. The mean of the eigenvalues for all the synthesized images is also plotted ($\bar{\lambda_s}$) and it is found to be in close proximity to the experimental data points, λ_e, for all three cases. To study the UQ problem for the reconstructed microstructures, five different parameters are derived from the PEM map.

The first parameter is the *radius* (R) of the enclosed circle that completely covers the cluster of all synthesized eigenvalue points where the center of the circle is defined as the eigenvalue of the experimental image (λ_e). The radius parameter measures the maximum possible extent of the data spread in the eigenspace with respect to the experimental value.

The second parameter is the *average distance* ($d_{\bar{\lambda}}$), which measures the distance between the average eigenvalue of all synthesized images ($\bar{\lambda_s}$) and the eigenvalue of the experimental image (λ_e). $d_{\bar{\lambda}}$ helps in evaluating the average of the data spread for a given reconstruction procedure. This is because the PEM of an image as a whole predominantly depends on the image size and the pixel area, which is the sum of all pixel intensities of all three color channels (Red–Green–Blue). However, the ratio of the radius over this average distance can distinguish different images vividly.

$$d_{\bar{\lambda}} = \|\bar{\lambda_s} - \lambda_e\| \tag{13}$$

The next parameter, ζ, is the mean of the distances between all the synthesized points with respect to the experimental eigenvalue. ζ is defined to demonstrate the statistical similarity of 2D and 3D reconstructed microstructures to the experimental data where N stands for the total number of synthesized samples.

$$\zeta = \frac{\sum(\|\lambda_s - \lambda_e\|)}{N} \tag{14}$$

The last two parameters, ρ_a and ρ_p are the ratios of the area and perimeter of the enclosed circle to that of a convex hull. The circle covers the maximum area enclosed by the spread of all the λ_s points. On the other hand, the convex hull is the closure of the smallest area covered by the spread of all the λ_s points.

$$\rho_a = \frac{\text{Area of the enclosed circle}}{\text{Area of the convex hull}} \tag{15}$$

$$\rho_p = \frac{\text{Perimeter of the enclosed circle}}{\text{Perimeter of the convex hull}} \tag{16}$$

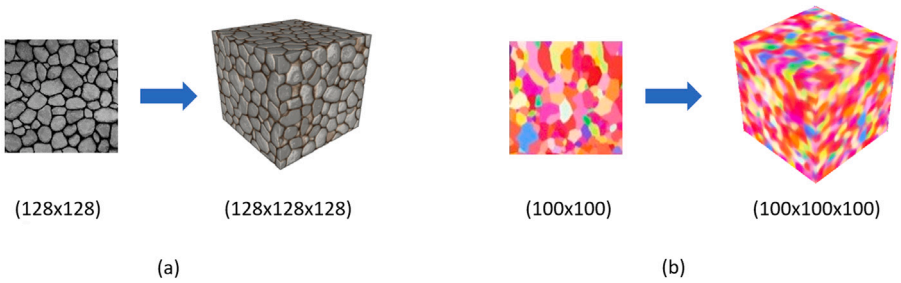

Fig. 4. (a) Original and reconstructed 3D microstructures of the cobblestone image, (b) Original and reconstructed 3D microstructures of forged Ti-7Al image.

Table 2
Developed metrics for statistical quantification of 3D microstructure samples.

	R			d_λ		
	X	Y	Z	X	Y	Z
Cobblestone	0.1317	0.1694	0.1518	0.0602	0.0564	0.0567
Forged	0.1024	0.1057	0.0905	0.0303	0.0335	0.0291

One can use these five parameters to investigate the uncertainty of the reconstructed samples. In this study, the additively manufactured microstructure images are expected to demonstrate higher variations in microstructural features due to their complex grain shapes [69]. This hypothesis is also verified using the radius parameter defined above. However, the high ρ_a value computed for the additively manufactured microstructure reveals that the level of uncertainty associated with each reconstruction is different. These calculations show that the synthesized image may differ significantly from the experimental image due to the epistemic uncertainty.

According to the comparison provided in Table 1, the reconstruction of cobblestone is found to be more robust than the other examples. This also implies that if the statistical information available for the input image is sufficient, MRF can generate images at larger scales, irrespective of the image size.

	ζ		
	X	Y	Z
Cobblestone	0.0684	0.0644	0.0640
Forged	0.0509	0.0453	0.0428

	ρ_a			ρ_p		
	X	Y	Z	X	Y	Z
Cobblestone	4.8099	7.7365	9.6451	1.9377	2.3866	2.4066
Forged	4.3381	4.2662	2.8814	1.7343	1.9250	1.6044

5. Uncertainty quantification for 2D-to-3D microstructure reconstruction

While comparing 2D and 3D samples is more challenging, it is still possible using PEM. The same set of five parameters is used here as well to quantify the uncertainty in microstructural features and show the statistical similarity of the reconstructed microstructures to the input samples. Two cases of synthesized microstructures are reported here using MRF with isotropic reconstruction (the 3D microstructure is build upon the plane sections that are consisted of the same 2D input sample) (Fig. 4).

For example, a 2D image of cobblestone is reconstructed using the MRF technique to obtain a 3D microstructure (Fig. 4(a)). Each stone and the gap separating them in the 2D image and 3D structure are assumed to represent a grain and grain boundary of a microstructure. The grain boundary thickness is defined for the 3D microstructure to have a separate cluster of 3D shapes.

For illustration, a microstructure image of the forged Ti-7Al is used to reconstruct a 3D microstructure using the MRF approach. However, unlike the previous example of the cobblestone, each voxel here contains three sets of values representing the color intensity values of Red–Green–Blue (RGB) channels. The MRF technique applies a voxel-by-voxel filling approach based on matching the neighbor window of a voxel with the 2D image locally in addition to using a global optimization approach, as discussed in Ref. [11]. Therefore, it is important to include each pixel and voxel value while comparing the 2D and 3D microstructures to understand if the reconstructed data is statistically equivalent to the input 2D data. The eigenvalues for all the plane-sections normal to X, Y, and Z directions are calculated and plotted in the PEM map (Fig. 5(a–f)). However, the data points of the 3D reconstructed microstructure are located within a range around the original eigenvalues of the input 2D image. This proves that the reconstructed sample is statistically similar to the input data which can also be observed in Table 2.

The histogram of PEM for 1000 synthesized microstructures demonstrates a normal distribution (Fig. 2) as MRF uses a Gaussian distributed weight parameter to determine the probability information. This result is significant since the Gaussian-distributed features can be used to model uncertainty propagation (on material properties) using linear transformation or Gaussian Process Regression (GPR). The PEM, on the other hand, does not have a linear relationship with the material characteristics.

6. Uncertainty quantification for homogenized mechanical properties

To study the propagation of the uncertainty on homogenized mechanical properties, the reconstruction is performed for the additively manufactured microstructures (Fig. 1(c)) by generating 1000 samples for 2D and 10 samples for 3D domains. The epistemic uncertainty arising from the reconstruction propagates on the microstructure, as reflected by the variations in the grain shapes. This microstructural uncertainty can also propagate on homogenized properties. To compute the variations in properties, crystal plasticity behavior is simulated using PRISMS plasticity [70]. Uniaxial tension simulations are performed for the 2D and 3D microstructures as presented in Fig. 6.

6.1. Quasi-linearity assumption

In the first application, the grain shape descriptors and material properties are assumed to involve a quasi-linear relationship to apply an analytical UQ algorithm [26–28,71–73]. This is because the analytical algorithm utilizes the linear transformation feature of the Gaussian distribution that captures the variations in the eigenvalue descriptors.

In particular, the analytical method solves for the expected values and covariance of the outputs using Eqs. (17) and (18) by assuming that the inputs are Gaussian distributed:

$$[a]_{2x2}[\mu_\lambda]_{2x1} = [\mu_M]_{2x1} \tag{17}$$

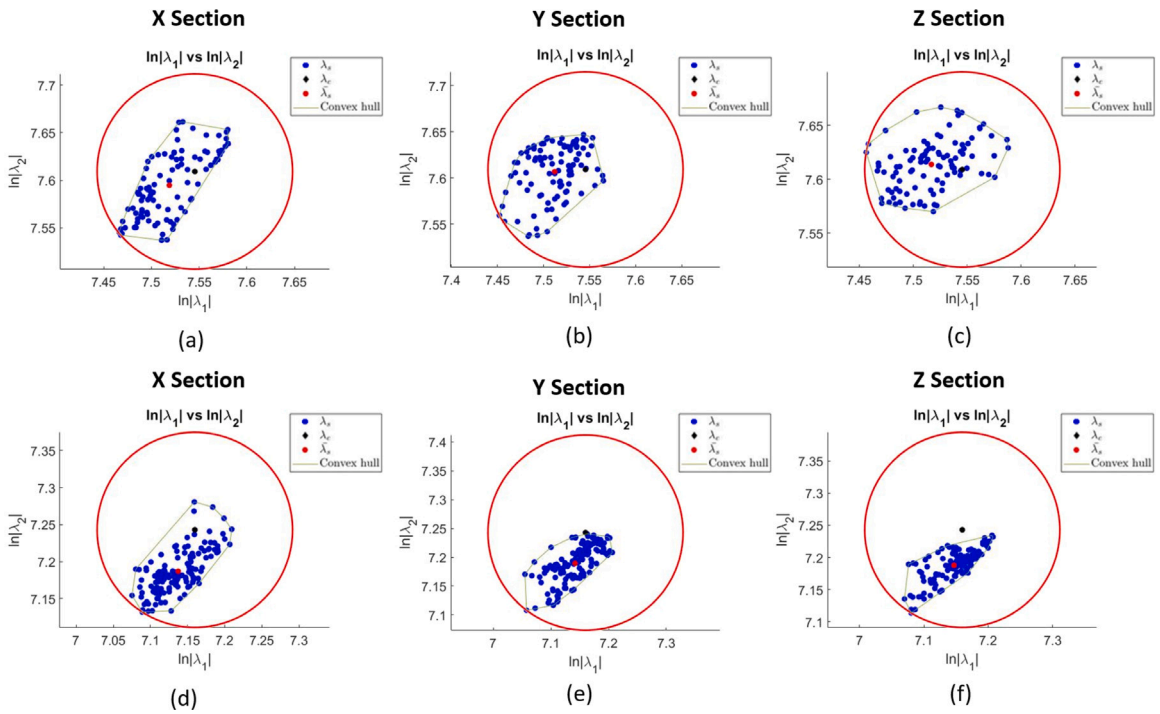

Fig. 5. (a)–(c) Eigenspace for X, Y and Z sections of 3D forged Ti-7Al microstructure, (d)–(f) Eigenspace for X, Y and Z sections of 3D cobblestone.

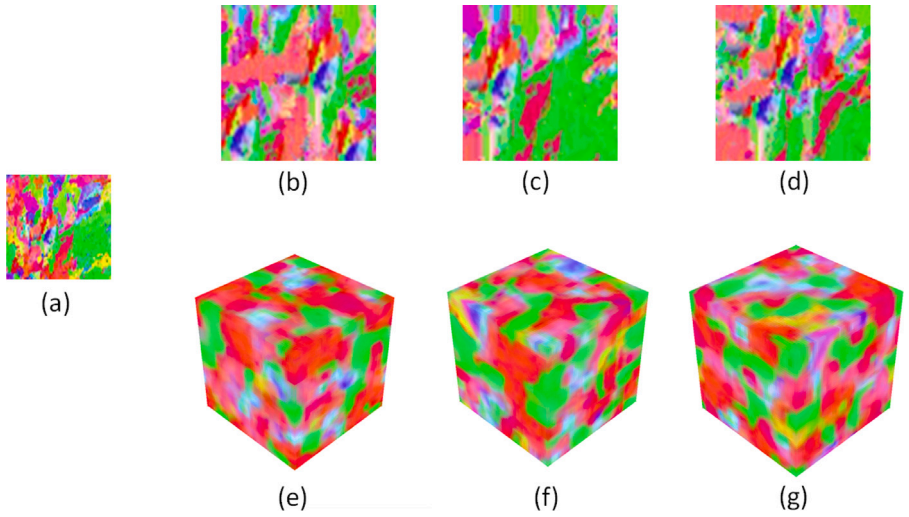

Fig. 6. (a) Experimental image; (b)–(d) 2D reconstructed microstructures; (e)–(g) 3D reconstructed microstructures.

$$[a]_{2x2}[\Sigma_\lambda]_{2x2}[a^T]_{2x2} = [\Sigma_M]_{2x2} \tag{18}$$

where μ_λ and Σ_λ represent the expected values vector and covariance matrix for the eigenvalue descriptors, a is the constant values vector that defines the presumed quasi-linear relationship between the grain shape description and homogenized properties, defined by the vector of M.

The variations in the microstructural features quantified by PEM and computed homogenized Young's modulus and yield strength values are plotted in Fig. 7. The standard deviations computed for the synthesized 2D and 3D microstructures are shown in Tables 3 and 4. Note that the standard deviation is calculated using the real mean (of the experimental microstructure) instead of the population mean (mean value of reconstructed samples). For a better representation, the absolute value of the natural logarithm of PEM is plotted. For 3D microstructures, PEM is calculated for each cross section in all three X, Y, and Z directions.

The difference in standard deviations of PEM representing the 2D image (Table 3) and the 3D reconstructed microstructures (Table 4) are found to be low. However, this small difference leads to a significant change in the standard deviation of the mechanical properties. The reason for the uncertainty propagation on properties is due to the randomness of the MRF algorithm and the erroneous pixel intensity values of the input experimental image. Even though the MRF can amplify the uncertainty due to an imperfect image resolution, it is crucial to maintain its algorithmic stochasticity to represent the inherent material uncertainty. However, the quality of experimental microstructure images can be improved through a smoothing algorithm that averages the distribution of the pixel intensity.

The experimental data is plotted in the black vertical dash line (Figs. 7 and 8) The red vertical dash line is representing the mean

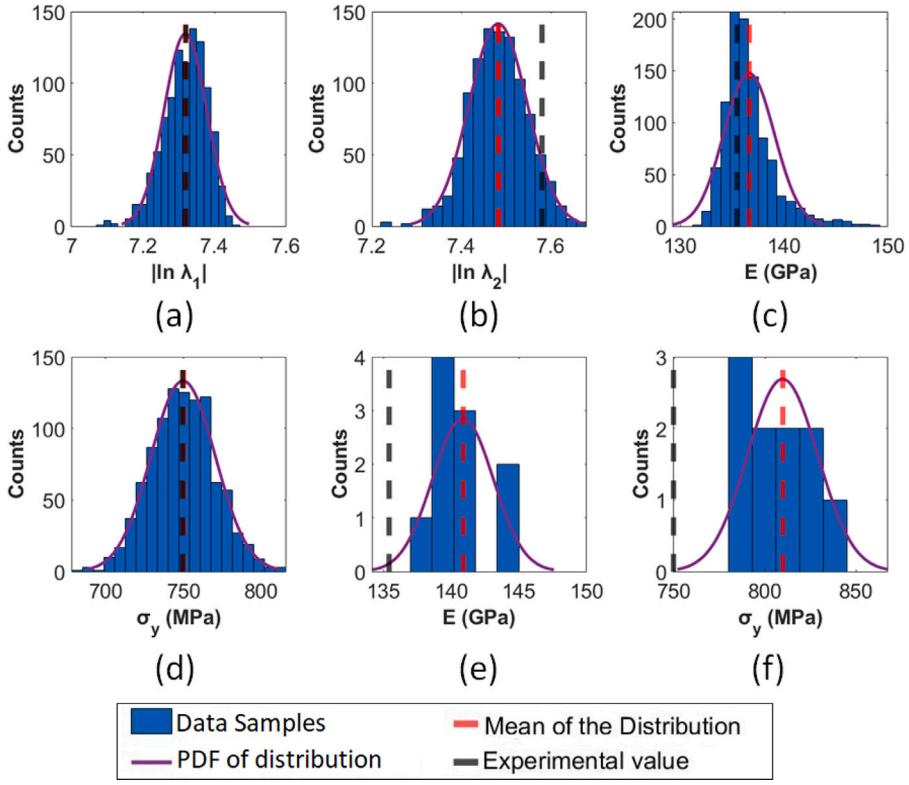

Fig. 7. (a)–(b) Distribution of PEM quantifying the 2D reconstructed microstructure images; (c)–(d) Distribution of material properties of the 2D reconstructed microstructures; (e)–(f) Distribution of material properties of the 3D reconstructed microstructures.

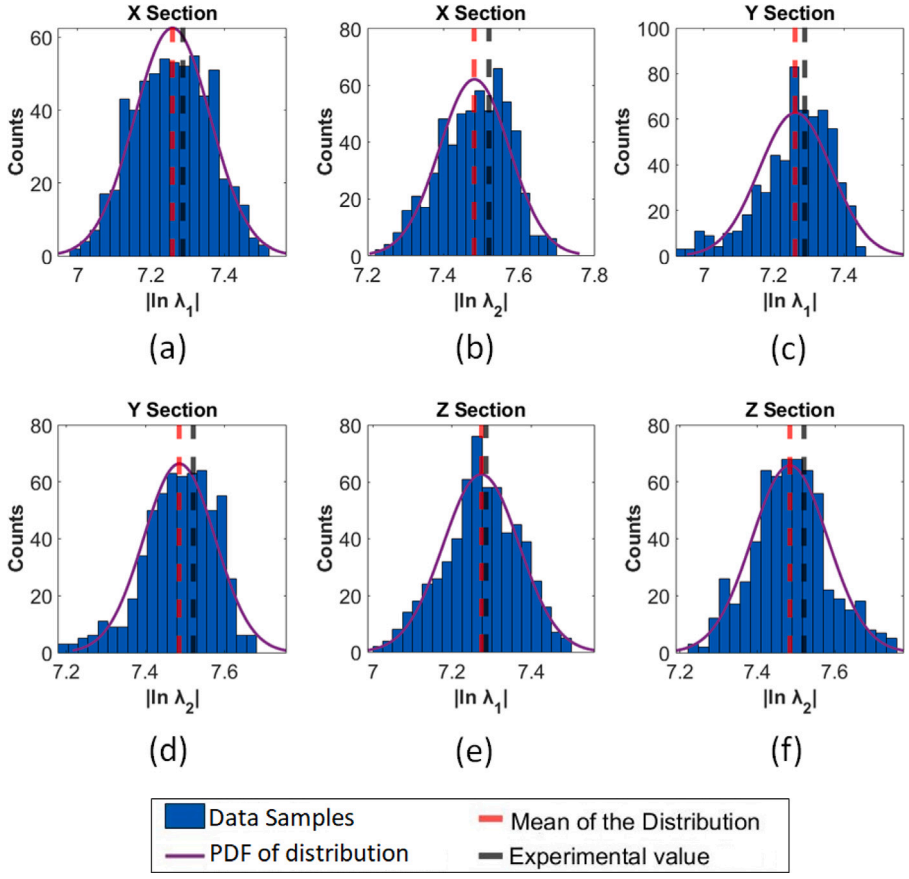

Fig. 8. (a)–(b) Distribution of λ_1 and λ_2 for the 3D additively manufactured microstructure cross sections in x direction, (c)–(d) Distribution of λ_1 and λ_2 for the 3D additively manufactured microstructure cross sections in y direction, (e)–(f) Distribution of λ_1 and λ_2 for the 3D additively manufactured microstructure cross sections in z direction.

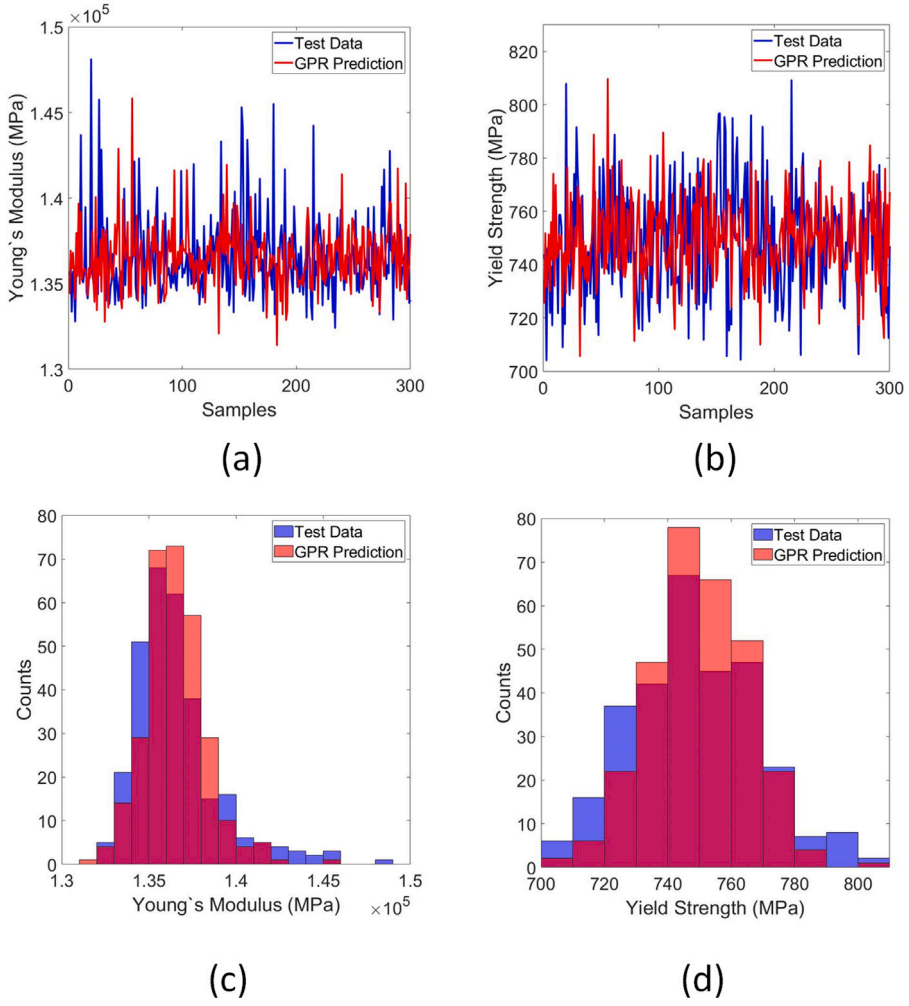

Fig. 9. (a)–(b) GPR predictions and test data for Young's modulus and yield strength respectively, (c)–(d) Probability distributions of 2D additively manufactured microstructures for Young's modulus and yield strength respectively.

Table 3
Standard deviation of different distributions of 2D microstructures.

	λ_1	λ_2	E (GPa)	σ_Y (MPa)
2D	0.0594	0.1176	2.7108	20.6666

value obtained from the reconstructed microstructures. The differences between these two mean values are associated with the epistemic uncertainty of MRF.

Finally, the probability distributions for the microstructural cross-sections of the 3D domain are shown in Fig. 8. Similarly, the experimental data is plotted in the black vertical dash line. The red vertical dash line shows the mean value obtained from the reconstructed microstructures.

6.2. Non-linearity assumption

By acknowledging that the relationship between the microstructure and homogenized properties can be nonlinear, the Gaussian Process Regression (GPR) is employed using the kriging method [74–77]. With the use of the GPR method, the covariance of the outcomes is automatically predicted in addition to the mean value estimations. Therefore, it leads to an efficient approach to study the uncertainty propagation on outputs. In this study, the DACE toolbox is utilized to build the kriging model [78]

A Gaussian Process is a collection of random variables that agree with a joint Gaussian probability function [79]. Here, the mechanical properties, such as Young's modulus and yield strength, are defined as a function of the microstructures represented by the PEM without normalization. Kriging model uses a second-order polynomial regression along with the following exponential correlation function to predict the mechanical properties.

$$corr(X_i, X_j) = \prod e^{-\theta_{jk}|X_{ik}, X_{jk}|} \tag{19}$$

where θ is the hyper-parameter which is obtained with a minimum error strategy between test points and predictions. Eq. (19) measures the correlation between the (X_{ik}) and (X_{jk}). The kriging surrogate model is developed using 70% of the data samples for training and 30% of the data samples for test.

The predictions of the surrogate model are illustrated in Fig. 9. The predictions indicate an average error of 2.1719 GPa and 20.0685 MPa for Young's modulus and yield strength, respectively. The probability distributions of the test data and kriging predictions given in Fig. 9 demonstrate a good match.

The similarity between the GPR-predicted outcomes and test data (Fig. 9(a) and (b)) implies that the link between the material properties and PEM may agree an exponential relationship.

Table 4
Standard deviation of different distributions of 3D microstructures.

	λ_1			λ_2			E	σ_Y
	X	Y	Z	X	Y	Z		
3D	0.1070	0.1004	0.1061	0.0969	0.0963	0.1051	6.1456	66.3130

7. Conclusion

This work proposes Principal Eigenvalue Moments (PEM) based on Hu moments as a descriptor to quantify the uncertainty of microstructural features and homogenized properties arising from the computational reconstruction of the synthetic samples. A graphical map based on PEM is developed to statistically validate the synthesized data of 2D and 3D reconstruction and quantify the uncertainty. Five different parameters are derived from the graphical map to understand and analyze the quality of the reconstruction. The propagation of the uncertainty on homogenized mechanical properties is studied under two assumptions based on the relationship between the PEM and mechanical properties (i.e., Young's modulus and yield strength). The quasi-linear assumption employs an analytical UQ algorithm to find the uncertainty of properties by utilizing the linear transformation feature of the Gaussian-distributed microstructural features. The non-linearity assumption predicts the uncertainty of properties by developing a GPR-based surrogate model as a function of the PEM. In the future work, the presented five parameters may be extended to analyze the uncertainty arising from the 3D to 3D reconstruction of additively manufactured microstructures.

CRediT authorship contribution statement

Arulmurugan Senthilnathan: Conceptualization, Methodology, Writing – original draft, Writing – review & editing. **Iman Javaheri:** Conceptualization, Writing – original draft, Writing – review & editing. **Hengduo Zhao:** Conceptualization, Writing – original draft, Writing – review & editing. **Veera Sundararaghavan:** Conceptualization, Writing – original draft, Writing – review & editing. **Marc DeGraef:** Conceptualization, Writing – original draft, Writing – review & editing. **Pınar Acar:** Conceptualization, Writing – original draft, Writing – & review & editing, Supervision.

Declaration of competing interest

The authors declare the following financial interests/personal relationships which may be considered as potential competing interests:Pinar Acar and Arulmurugan Senthilnathan reports financial support was provided by Air Force Office of Scientific Research (AFOSR) Young Investigator Program under Grant FA9550-21-1-0120. Veera Sundararaghavan and Iman Javaheri reports financial support was provided by National Science Foundation Graduate Research Fellowship Program (Grant No. DGE 1841052). Pinar Acar andHengduo Zhao reports financial support was provided by Commonwealth Center for Advanced Manufacturing under innovation program, E-084. The authors acknowledge Professor John Allison from Department of Material Science and Engineering at University of Michigan, Ann Arbor for kindly providing the experimental images.

Data availability

Data will be made available on request.

Acknowledgments

The authors acknowledge Professor John Allison from Department of Material Science and Engineering at University of Michigan, Ann Arbor for kindly providing the experimental images. IJ and VS would like to acknowledge the National Science Foundation Graduate Research Fellowship Program (Grant No. DGE 1841052) for financial support. PA and AS acknowledge financial support from the Air Force Office of Scientific Research (AFOSR) Young Investigator Program under Grant FA9550-21-1-0120. PA and HZ acknowledge the support from Commonwealth Center for Advanced Manufacturing under innovation program, E-084.

References

[1] Mark D. Rintoul, Salvatore Torquato, Reconstruction of the structure of dispersions, J. Colloid Interface Sci. 186 (2) (1997) 467–476.
[2] C. Yeong, S. Torquato, Reconstructing random media, Phys. Rev. E 57 (1) (1998) 495.
[3] C. Yeong, S. Torquato, Reconstructing random media. II. Three-dimensional media from two-dimensional cuts, Phys. Rev. E 58 (1) (1998) 224.
[4] David M. Saylor, Joseph Fridy, Bassem S. El-Dasher, Kee-Young Jung, Anthony D. Rollett, Statistically representative three-dimensional microstructures based on orthogonal observation sections, Metall. Mater. Trans. A 35 (7) (2004) 1969–1979.
[5] Niall Sheehan, S. Torquato, Generating microstructures with specified correlation functions, J. Appl. Phys. 89 (1) (2001) 53–60.
[6] Yu Liu, M. Steven Greene, Wei Chen, Dmitriy A. Dikin, Wing Kam Liu, Computational microstructure characterization and reconstruction for stochastic multiscale material design, Comput. Aided Des. 45 (1) (2013) 65–76.
[7] Ali Hasanabadi, Majid Baniassadi, Karen Abrinia, Masoud Safdari, Hamid Garmestani, 3D microstructural reconstruction of heterogeneous materials from 2D cross sections: A modified phase-recovery algorithm, Comput. Mater. Sci. 111 (2016) 107–115.
[8] David T. Fullwood, Stephen R. Niezgoda, Surya R. Kalidindi, Microstructure reconstructions from 2-point statistics using phase-recovery algorithms, Acta Mater. 56 (5) (2008) 942–948.
[9] Hongyi Xu, Dmitriy A. Dikin, Craig Burkhart, Wei Chen, Descriptor-based methodology for statistical characterization and 3D reconstruction of microstructural materials, Comput. Mater. Sci. 85 (2014) 206–216.
[10] Veeraraghavan Sundararaghavan, Nicholas Zabaras, Classification and reconstruction of three-dimensional microstructures using support vector machines, Comput. Mater. Sci. 32 (2) (2005) 223–239.
[11] Iman Javaheri, Veera Sundararaghavan, Polycrystalline microstructure reconstruction using Markov random fields and histogram matching, Comput. Aided Des. 120 (2020) 102806.
[12] Iman Javaheri, Mohsen Taheri Andani, Veera Sundararaghavan, Large-scale synthesis of metal additively-manufactured microstructures using markov random fields, Comput. Mater. Sci. 206 (2022) 111228.
[13] Pinar Acar, Veera Sundararaghavan, A Markov random field approach for modeling spatio-temporal evolution of microstructures, Modelling Simulation Mater. Sci. Eng. 24 (7) (2016) 075005.
[14] Veera Sundararaghavan, Reconstruction of three-dimensional anisotropic microstructures from two-dimensional micrographs imaged on orthogonal planes, Integr. Mater. Manuf. Innov. 3 (1) (2014) 19.
[15] A. Kumar, L. Nguyen, M. DeGraef, V. Sundararaghavan, A Markov random field approach for microstructure synthesis, Modelling Simulation Mater. Sci. Eng. 24 (3) (2016) 035015.
[16] Ramin Bostanabad, Reconstruction of 3D microstructures from 2D images via transfer learning, Comput. Aided Des. 128 (2020) 102906.
[17] Anindya Bhaduri, Ashwini Gupta, Audrey Olivier, Lori Graham-Brady, An efficient optimization based microstructure reconstruction approach with multiple loss functions, Comput. Mater. Sci. 199 (2021) 110709.
[18] Ramin Bostanabad, Anh Tuan Bui, Wei Xie, Daniel W. Apley, Wei Chen, Stochastic microstructure characterization and reconstruction via supervised learning, Acta Mater. 103 (2016) 89–102.

[19] Xiaolin Li, Yichi Zhang, He Zhao, Craig Burkhart, L. Catherine Brinson, Wei Chen, A transfer learning approach for microstructure reconstruction and structure–property predictions, Sci. Rep. 8 (1) (2018) 1–13.

[20] Jinlong Fu, Dunhui Xiao, Dongfeng Li, Hywel R. Thomas, Chenfeng Li, Stochastic reconstruction of 3D microstructures from 2D cross-sectional images using machine learning-based characterization, Comput. Methods Appl. Mech. Engrg. 390 (2022) 114532.

[21] Anh Tran, Hoang Tran, Data-driven high-fidelity 2D microstructure reconstruction via non-local patch-based image inpainting, Acta Mater. 178 (2019) 207–218.

[22] T.J. Turner, et al., The influence of microstructure on surface strain distributions in a nickel micro-tension specimen, Modelling Simul. Mater. Sci. Eng. 21 (2013) 015002.

[23] Nicolas, et al., Reconstruction methods and analysis of subsurface uncertainty for anisotropic microstructures, Mater. Sci. Eng. A 760 (2019) 76–87.

[24] A. Brahme, M.H. Alvi, D. Saylor, J. Fridy, A.D. Rollett, 3D reconstruction of microstructure in a commercial purity aluminum, Scr. Mater. 55 (1) (2006) 75–80.

[25] Sriram Ganesan, Iman Javaheri, Veera Sundararaghavan, Constrained voronoi models for interpreting surface microstructural measurements, Mech. Mater. 159 (2021) 103892.

[26] Acar Pınar, Uncertainty quantification for Ti-7Al alloy microstructure with an inverse analytical model (AUQLin), Materials 12 (11) (2019) 1773.

[27] Acar Pınar, Veera Sundararaghavan, Uncertainty quantification of microstructural properties due to variability in measured pole figures, Acta Mater. 124 (2017) 100–108.

[28] Pinar Acar, Veera Sundararaghavan, Uncertainty quantification of microstructural properties due to experimental variations, AIAA J. 55 (8) (2017) 2824–2832.

[29] Pinar Acar, Machine learning reinforced crystal plasticity modeling under experimental uncertainty, AIAA J. 58 (8) (2020) 3569–3576.

[30] Arulmurugan Senthilnathan, Pinar Acar, Shape moment invariants as a new methodology for uncertainty quantification in microstructures, in: AIAA Scitech 2021 Forum, 2021.

[31] P.G. Callahan, M. Groeber, M. De Graef, Towards a quantitative comparison between experimental and synthetic grain structures, Acta Mater. 111 (2016) 242–252.

[32] B.J. Inkson, M. Mulvihill, G. Möbus, 3D determination of grain shape in a FeAl-based nanocomposite by 3D FIB tomography, Scr. Mater. 45 (7) (2001) 753–758.

[33] Melissa R. Cox, Muniram Budhu, A practical approach to grain shape quantification, Eng. Geol. 96 (1–2) (2008) 1–16.

[34] Abhik Choudhury, Yuksel C. Yabansu, Surya R. Kalidindi, Anne Dennstedt, Quantification and classification of microstructures in ternary eutectic alloys using 2-point spatial correlations and principal component analyses, Acta Mater. 110 (2016) 131–141.

[35] Ahmet Cecen, Tony Fast, Surya R. Kalidindi, Versatile algorithms for the computation of 2-point spatial correlations in quantifying material structure, Integr. Mater. Manuf. Innov. 5 (1) (2016) 1–15.

[36] A. Tewari, A.M. Gokhale, J.E. Spowart, D.B. Miracle, Quantitative characterization of spatial clustering in three-dimensional microstructures using two-point correlation functions, Acta Mater. 52 (2) (2004) 307–319.

[37] Ramin Bostanabad, Yichi Zhang, Xiaolin Li, Tucker Kearney, L. Catherine Brinson, Daniel W. Apley, Wing Kam Liu, Wei Chen, Computational microstructure characterization and reconstruction: Review of the state-of-the-art techniques, Prog. Mater. Sci. 95 (2018) 1–41.

[38] S. Torquato, Random Heterogeneous Materials: Microstructure and Macroscopic Properties, Springer Verlag, New York, 2002.

[39] J. MacSleyne, M.D. Uchic, J.P. Simmons, M. De Graef, Three-dimensional analysis of secondary γ' precipitates in René-88 DT and UMF-20 superalloys, Acta Mater. 57 (20) (2009) 6251–6267.

[40] Dongming Zhao, Jie Chen, Affine curve moment invariants for shape recognition, Pattern Recognit. 30 (6) (1997) 895–901.

[41] Paul L. Rosin, Measuring shape: ellipticity, rectangularity, and triangularity, Mach. Vis. Appl. 14 (3) (2003) 172–184.

[42] Patrick Gregory Callahan, Quantitative Characterization and Comparison of Precipitate and Grain Shape in Nickel-Base Superalloys using Moment Invariants (Diss.), Carnegie Mellon University, 2012.

[43] P.G. Callahan, J.P. Simmons, M. De Graef, A quantitative description of the morphological aspects of materials structures suitable for quantitative comparisons of 3D microstructures, Modelling Simulation Mater. Sci. Eng. 21 (1) (2012) 015003.

[44] Jeremiah P. MacSleyne, Moment Invariants for 2-D and 3-D Characterization of the Morphology of Gamme-Prime Precipitates in Nickel-Base Superalloys (Ph.D. thesis), Carnegie Mellon University, 2008.

[45] J.P. MacSleyne, J.P. Simmons, M. De Graef, On the use of 2-D moment invariants for the automated classification of particle shapes, Acta Mater. 56 (3) (2008) 427–437.

[46] J.P. MacSleyne, J.P. Simmons, M. De Graef, On the use of moment invariants for the automated analysis of 3D particle shapes, Modelling Simulation Mater. Sci. Eng. 16 (4) (2008) 045008.

[47] M.A.R.C. DeGRAEF, AFRL-AFOSR-VA-TR-2016-0040.

[48] Felix Schleifer, Moritz Müller, Yueh-Yu Lin, Markus Holzinger, Uwe Glatzel, Michael Fleck, Consistent quantification of precipitate shapes and sizes in two and three dimensions using central moments, Integr. Mater. Manuf. Innov. (2022) 1–13.

[49] Lily Nguyen, Rongpei Shi, Yunzhi Wang, Marc De Graef, Quantification of rafting of γ' precipitates in Ni-based superalloys, Acta Mater. 103 (2016) 322–333.

[50] Ming-Kuei Hu, Visual pattern recognition by moment invariants, IRE Trans. Inf. Theory 8 (2) (1962) 179–187.

[51] Muharrem Mercimek, Kayhan Gulez, Tarik Veli Mumcu, Real object recognition using moment invariants, Sadhana 30 (6) (2005) 765–775.

[52] Tejtasin Phiasai, Somchai Arunrungrusmi, Kosin Chamnongthai, Face recognition system with PCA and moment invariant method. ISCAS 2001, in: The 2001 IEEE International Symposium on Circuits and Systems (Cat. No. 01CH37196), Vol. 2, IEEE, 2001.

[53] Anant Bhardwaj, Manpreet Kaur, Anupam Kumar, Recognition of plants by leaf image using moment invariant and texture analysis, Int. J. Innov. Appl. Stud. 3 (1) (2013) 237–248.

[54] Yudong Zhang, Jianfei Yang, Shuihua Wang, Zhengchao Dong, Preetha Phillips, Pathological brain detection in MRI scanning via Hu moment invariants and machine learning, J. Exp. Theoret. Artif. Intell. 29 (2) (2017) 299–312.

[55] Yu-Dong Zhang, Yin Zhang, Yi-Ding Lv, Xiao-Xia Hou, Fang-Yuan Liu, Wen-Juan Jia, Meng-Meng Yang, Preetha Phillips, Shui-Hua Wang, Alcoholism detection by medical robots based on Hu moment invariants and predator–prey adaptive-inertia chaotic particle swarm optimization, Comput. Electr. Eng. 63 (2017) 126–138.

[56] Zhihu Huang, Jinsong Leng, Analysis of Hu's moment invariants on image scaling and rotation, in: 2010 2nd International Conference on Computer Engineering and Technology, Vol. 7, IEEE, 2010.

[57] Dragiša Žunić, Joviša Žunić, Shape ellipticity from Hu moment invariants, Appl. Math. Comput. 226 (2014) 406–414.

[58] Joviša Žunić, Kaoru Hirota, Dragan Dukić, Mehmet Ali Aktaş, On a 3D analogue of the first Hu moment invariant and a family of shape ellipsoidness measures, Mach. Vis. Appl. 27 (1) (2016) 129–144.

[59] Joviša Žunić, Kaoru Hirota, Paul L. Rosin, A Hu moment invariant as a shape circularity measure, Pattern Recognit. 43 (1) (2010) 47–57.

[60] Dragiša Žunić, Joviša Žunić, Shape ellipticity based on the first Hu moment invariant, Inform. Process. Lett. 113 (19–21) (2013) 807–810.

[61] Arulmurugan Senthilnathan, Pınar Acar, Marc De Graef, Markov Random Field based microstructure reconstruction using the principal image moments, Mater. Charact. 178 (2021) 111281.

[62] B. Hiriyur, H. Waisman, G. Deodatis, Uncertainty quantification in homogenization of heterogeneous microstructures modeled by XFEM, Internat. J. Numer. Methods Engrg. 88 (2011) 257–278.

[63] Shravan Kotha, Deniz Ozturk, Somnath Ghosh, Uncertainty-quantified parametrically homogenized constitutive models (UQ-PHCMs) for dual-phase α/β titanium alloys, Npj Comput. Mater. 6 (1) (2020) 1–20.

[64] Pejman Honarmandi, Raymundo Arróyave, Uncertainty quantification and propagation in computational materials science and simulation-assisted materials design, Integr. Mater. Manuf. Innov. 9 (1) (2020) 103–143.

[65] Rohit K. Tripathy, Ilias Bilionis, Deep UQ: Learning deep neural network surrogate models for high dimensional uncertainty quantification, J. Comput. Phys. 375 (2018) 565–588.

[66] C. Frederic Smith, Braden Lapp, Michael Glavicic, Uncertainty quantification of material mechanical properties using surrogate models, in: 17th AIAA/ISSMO Multidisciplinary Analysis and Optimization Conference, 2016.

[67] Ernst Ising, Beitrag zur theorie des ferromagnetismus, Z. Phys. 31 (1) (1925) 253–258.

[68] Jin Soo Noh, Kang Hyeon Rhee, Palmprint identification algorithm using Hu invariant moments and Otsu binarization, in: Fourth Annual ACIS International Conference on Computer and Information Science, ICIS'05, IEEE, 2005.

[69] Bradley H. Jared, Miguel A. Aguilo, Lauren L. Beghini, Brad L. Boyce, Brett W. Clark, Adam Cook, Bryan J. Kaehr, Joshua Robbins, Additive manufacturing: Toward holistic design, Scr. Mater. 135 (2017) 141–147.

[70] M. Yaghoobi, S. Ganesan, S. Sundar, A. Lakshmanan, S. Rudraraju, J.E. Allison, V. Sundararaghavan, PRISMS- Plasticity: An open-source crystal plasticity finite element software, Comput. Mater. Sci. 169 (2019) 109078.

[71] P. Acar, Recent progress of uncertainty quantification in small-scale materials science, Prog. Mater. Sci. 117 (2021) 100723.

[72] P. Acar, V. Sundararaghavan, Do epistemic uncertainties allow for replacing microstructural experiments with reconstruction algorithms? AIAA J. 57 (3) (2019) 1078–1091.

[73] P. Acar, Reliability based design optimization of microstructures with analytical formulation, J. Mech. Des. 140 (11) (2018) 111402.
[74] Noel Cressie, The origins of kriging, Math. Geol. 22 (3) (1990) 239–252, http://dx.doi.org/10.1007/BF00889887.
[75] Jay D. Martin, Timothy W. Simpson, Use of kriging models to approximate deterministic computer models, AIAA J. 43 (4) (2005) 853–863, http://dx.doi.org/10.2514/1.8650.
[76] Z. Wang, P. Liu, Y. Ji, S. Mahadevan, M.F. Horstemeyer, Z. Hu, L. Chen, L.Q. Chen, Uncertainty quantification in metallic additive manufacturing through physics-informed data-driven modeling, Jom 71 (8) (2019) 2625–2634, http://dx.doi.org/10.1007/s11665-014-0958-z.
[77] L. Xia, B. Raghavan, P. Breitkopf, Towards surrogate modeling of material microstructures through the processing variables, Appl. Math. Comput. 294 (2017) 157–168, http://dx.doi.org/10.1016/j.amc.2016.08.056.
[78] H.B. Nielsen, S.N. Lophaven, J. Søndergaard, DACE - a matlab kriging toolbox, 2002, in: Computer Programme, Informatics and Mathematical Modelling, Technical University of Denmark, DTU.
[79] Felipe A.C. Viana, Timothy W. Simpson, Vladimir Balabanov, Vasilli Toropov, Special section on multidisciplinary design optimization: metamodeling in multidisciplinary design optimization: how far have we really come? AIAA J. 52 (4) (2014) 670–690, http://dx.doi.org/10.2514/1.J052375.